ICSV13 - Vienna
The Thirteenth International Congress on Sound and Vibration
Vienna, Austria, July 2-6, 2006

CLOSER ESTIMATING OF LOWEST BAND GAP IN TERNARY LOCALLY RESONANT PHONONIC CRYSTALS

Gang Wang*[1], Lihui Shao[2], Yaozong Liu[1], Dianlong Yu[1] and Jihong Wen[1]

[1] Institute of Mechatronical Engineering, National University of Defense Technology
Changsha 410073, China
[2]Astronaut Center of China, Beijing 100094, China
wang-g@vip.sina.com (e-mail address of lead author)

Abstract

Based on better understanding of the lattice vibration modes, two simple spring-mass models are constructed in order to estimate the frequencies on both the lower and upper edges of the lowest locally resonant band gaps of both the two- and three-dimensional ternary locally resonant phononic crystals. The parameters of the models are given in a reasonable way based on the physical insight of the band gap mechanism. Both the lumped-mass methods and our models are used in the study of the influences of structural and the material parameters on frequencies on both edges of the lowest gaps of in the ternary locally resonant phononic crystals. The analytical estimations using our models and the theoretical predictions with the lumped-mass method are in good agreement. The heuristic models are helpful for better understanding of the locally resonant band gap mechanism, as well as better estimation of the band edge frequencies.

INTRODUCTION

In recent years, a great deal of work has been devoted to the study of the propagation of elastic or acoustic wave in periodic structures made of different materials[1-13], which have been named the phononic crystals (PCs)[1] by analogy with the photonic crystals[14,15] for electromagnetic waves. Because of the periodicity in such structures, there exist frequency ranges in which elastic waves are forbidden. This phenomenon can be of real interest because of the rich physics of elastic system, where the wave can have mixed longitudinal and transverse modes, and where a large contrast between the elastic parameters is allowed. A famous example is the locally resonant (LR) PCs consisting of very soft rubber[2,4-8,10,11] (with an elastic constant of five orders lower than common solids) and other components. These new materials are most likely to obtain the low-frequency gaps with structures of small dimensions, leading to promising applications such as low-frequency vibration/noise insulations.

The lumped-mass (LM) method[9,10,12] is employed in the study of two-dimensional

(2D) and three-dimensional (3D) ternary LR PCs in this paper. It has been concluded[10,12] that the LM method converges faster than the traditional techniques and its convergence is insensitive to the sharp variation of elastic constants on the interfaces inside PCs. This advantage was unique in comparison with other works[5,13] on the improvement of traditional methods.

Several analog models have been used in the research of the mechanism of low-frequency band gaps in the LR PCs[5-7,11]. A simple mechanical model of masses and springs was firstly used by Goffaux, *et.al.*[5,6] in order to fit the transmission spectra near the first resonant peak and the edges of the first band gap in a 2D ternary LR PCs. We also established a similar model in order to clarify the origin of the LR band gaps in a 2D binary LR PCs[11]. However, the parameters of these models[5,6,11] are just given, not calculated with reasonable method based on physical insights. Hirsekorn used a different simple model[7] to evaluate the frequencies on the lower edges of the band gaps in a 2D ternary LR PCs, where the parameters are derived with reasonable way. However, the thin rubber layers in arc shape are treated as simple equal-thickness flat ones in his model[7], and the model can only be used to simulate the lower edges of the band gaps with slight mismatches. Whether or no, Hirsekorn's work[7] does motivate the works in this paper.

In this paper, we restudied the lattice vibration modes that concerns the formation of the lowest LR band gaps of typical 2D[6] and 3D[2] ternary PCs with the LM method. Both them consist of lattice of heavy cores (Au cylinders or Pb spheres) coated with silicon rubber and immersed in epoxy. An additional analog model is constructed to represent the vibration modes at the upper edges of the LR band gap. The parameters of the two models are calculated based on clear understanding of the physical insight. The two models and the arithmetic of its parameters are validated with the LM method by changing the structural and material parameters of the 2D and 3D ternary LR PCs.

LATTICE VIBRATION MODES OF THE 2D AND 3D TERNARY LR PCS

Figure 1(a) illustrates the in-plane mode band structure of typical 2D ternary LR PCs[6] calculated with the lumped-mass method. The calculated lattice vibration modes at points L_1, $L_{2,3}$ and $L'_{2,3}$ in Fig. 1(a) are shown in Fig. 1(b-d).

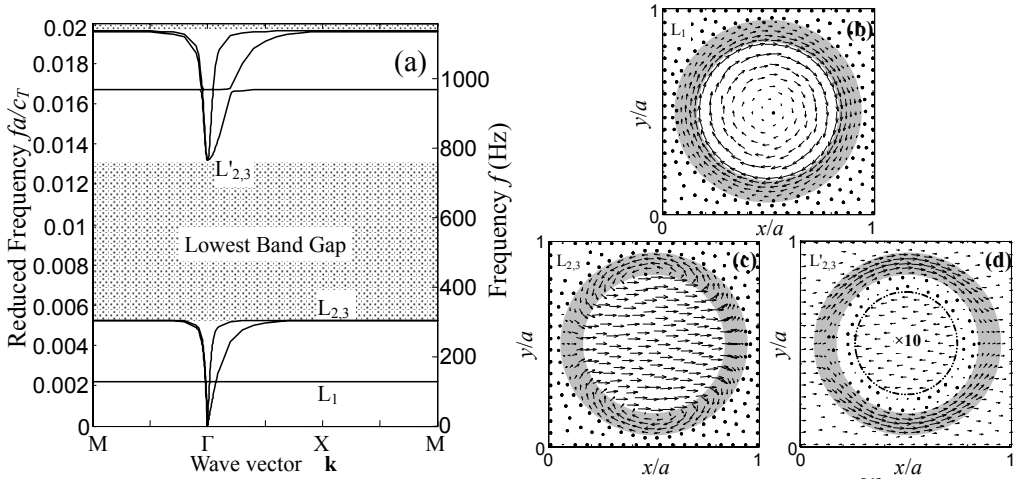

Figure 1 – (a)The in-plane mode band structure of typical 2D ternary LR PCs[6] which consist of square array of coated Au cylinders immersed in epoxy. The shadowed region represents the lowest band gap. (b,c,d) Lattice displacement vectors in the 2D ternary LR PCs corresponding to

(b)L_1, (c)$L_{2,3}$ and (d)$L'_{2,3}$ in Fig. 1(a), respectively. The direction and the length of each arrow represent the direction and amplitude of the displacement vector at the starting point of the arrow. The shadowed region, the inside and the outside represent the coating rubber, the Au core and the epoxy host respectively. The displacement vectors in the zone surrounded by dasheddotted line in Fig. (d) are magnified 10 times.

The clockwork-like torsion vibration mode illustrated in Fig. 1(b) is similar to the first LR mode[11] in the 2D binary LR PCs, which can hardly interact with the traveling waves with long wavelength in the host media, and for the same reason[11] no gap is generated.

The lowest LR band gap in the 2D ternary LR PCs is generated by the second and third LR modes illustrated in Fig. 1(c) where the Au core vibrates as one particle and the composition of the forces from the oscillator to the host media generates the lowest band gap at its eigenfrequency.

The two vibration modes at $L'_{2,3}$ (the upper edge of the lowest band gap) are similar with their corresponding LR modes at $L_{2,3}$, while the vibration of the host media is also involved and in the reversed phase with that of the core. The corresponding wave vector locates at point Γ, which means that the vibrations in adjacent lattice are in same phase.

We made similar studies on the typical 3D ternary LR PCs[2]. Figure 2 illustrates the calculated band structure of it and Fig. 3 illustrates the lattice vibration modes corresponding to points $L_{1,2,3}$, $L_{4,5,6}$ and $L'_{4,5,6}$ in Fig. 2.

Same clockwork-like torsion LR mode that cannot generate a gap is illustrated in Fig. 3(a). The lowest LR band gap in 3D ternary LR PCs is generated by the 4-6th LR modes $L_{4,5,6}$ that is combined together and illustrated in Fig. 3(b). The corresponding lattice vibration mode is almost the same with that illustrated in Fig. 1(c), i.e. the core vibrates conformably as one particle and the coating acting as springs. Other three vibration modes at $L'_{4,5,6}$ in Fig. 2 illustrated in Fig. 3(c) (at the upper edge of the lowest band gap) are similar with their corresponding LR modes at $L_{4,5,6}$.

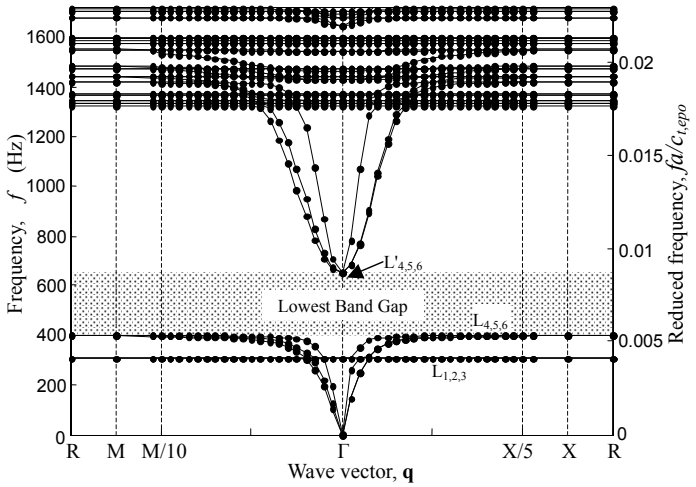

Figure 2 –The band structure of typical 3D[2] ternary LR PCs that consist of simple cubic arrays of coated Pb spheres immersed in epoxy. The shadowed region represents the lowest band gap.

ANALOG MODELS AND CALCULATION OF PARAMETERS OF IT

Based on above discussions, we can conclude that: (1) The vibration modes on the lower

edge of the lowest band gaps in both the 2D and the 3D LR PCs correspond to the mass-spring model illustrated in Fig. 4(d). (2) The vibration modes on the upper edge of the lowest band gaps in both the 2D and the 3D LR PCs can be described with a new "mass-spring-mass" model illustrated in Fig. 4(e). In the model, the new particles m_2 represents the equivalent mass of host media in a lattice.

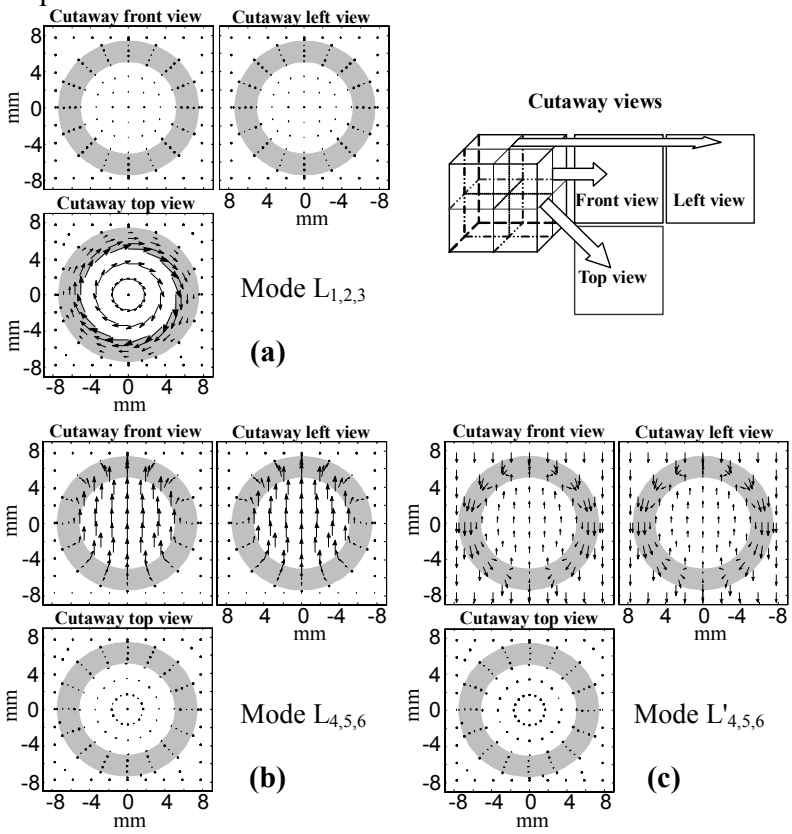

Figure 3 –Lattice displacement vectors in three perpendicular cutaway interfaces inside the 3D ternary LR PCs corresponding to (a)$L_{1,2,3}$, (b)$L_{4,5,6}$ and (c)$L'_{4,5,6}$ in Fig. 2 respectively. The direction and the length of each arrow represent the direction and amplitude of the displacement vector at the starting point of the arrow. The shadowed region, the inside and the outside represent the coating rubber, Pb core and epoxy host respectively.

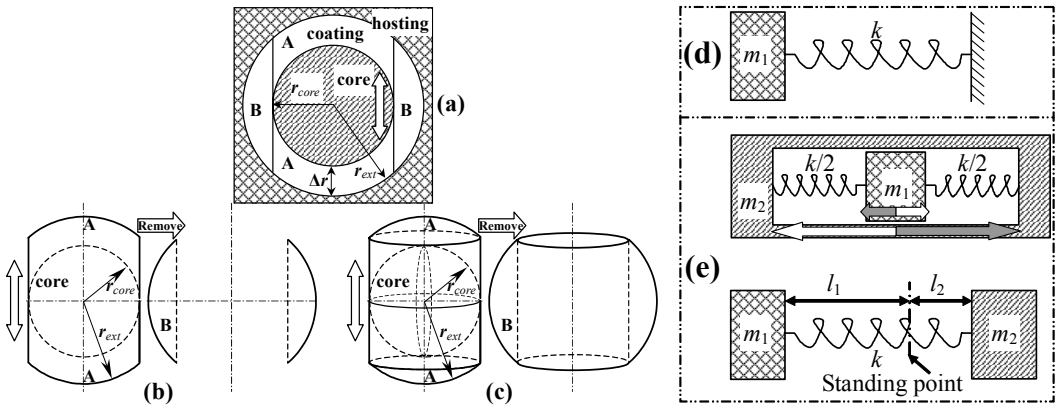

Figure 4 – (a) The cross section of the 2D and 3D ternary LR PCs. (b)(c) Sketch maps explaining the calculation methods of parameters in the analog models corresponding 2D and 3D ternary LR PCs respectively.(d,e)Analog models corresponding to vibration modes on the (d)lower and (e)upper edges of the lowest LR band gap.

As the phenomena of the 2D and 3D ternary LR PCs around the lowest band gap can be easily described with the sample models in Figs. 4(d) and 4(e), they may be used to evaluate the frequencies on the edges of the lowest band gap. This evaluation is much helpful for the simplification of the design of the LR PCs. However, accurate evaluations need the correct calculation of the parameters in the analog models. Here, three calculation methods are engaged and compared in the evaluation of frequencies of the lowest band gaps in 2D and 3D ternary LR PCs.

Based on the detailed vibration modes illustrated in Figs. 1(c), 1(d), 3(b) and 3(c), we can see that only rubbers in region A (illustrated in Fig. 4(a-c)) are mainly compressed and stretched when the core vibrates up and down. So stiffness k in Fig. 2 can be calculated with parameters in region A.

Hirsekorn-like method[7] is engaged as method I in this paper, where the m_1 and m_2 in Fig. 4(d-e) are considered as mass of the core and epoxy host in a lattice respectively and the rubber in region A is treated as two layers with equal-thickness Δr for simpleness. Thus, for the typical 2D ternary LR PCs,

$$m_1 = m_{core} = \rho_{core}\pi r_{core}^2;\ m_2 = m_{host} = \rho_{host}(a^2 - \pi r_{ext}^2) \tag{1}$$

$$k = 4C_{11}r_{\text{core}}/(r_{\text{ext}} - r_{\text{core}}) \tag{2}$$

and for the typical 3D one,

$$m_1 = m_{core} = (4/3)\rho_{core}\pi r_{core}^3;\ m_2 = m_{host} = \rho_{host}(a^3 - (4/3)\pi r_{ext}^3) \tag{3}$$

$$k = 2C_{11}\pi r_{\text{core}}^2/(r_{\text{ext}} - r_{\text{core}}) \tag{4}$$

where $C_{11}=\lambda_{\text{coating}}+2\mu_{\text{coating}}$, λ_{coating} and μ_{coating} are the Lame constants of the rubber in the coating layer.

The frequencies on the edges of the lowest LR band gap can thus be evaluated with

$$f_1 = (2\pi)^{-1}\sqrt{k/m_1};\quad f_2 = (2\pi)^{-1}\sqrt{k(m_1+m_2)/(m_1m_2)} \tag{5}$$

Using method I and the analog models, we evaluate the frequencies of the lowest band gap in 2D and 3D ternary LR PCs with different structural and material parameters (dotted lines in Figs. 5-9) and compared them with that calculated with the LM method (solid lines with dots in Figs. 5-9).

From these figures, we can see that the frequencies evaluated with method I are higher than the therotical results, especially at the upper edge of the band gap. The analog models with parameters calculated with method I match with the 2D and 3D LR PCs basically only at the lower edges of their band gaps. These mismatches are due to the underestimate of k, i.e. the equivalent stiffness of coating layer in region A in Fig. 4(a-c). Hirsekorn's simplification where the rubber is treated as a layer with equal-thickness Δr is not accurate because that only the thickness (along the direction of wave propagation) in the coating layer at the center of region A is Δr, and it is longer than Δr at other parts in region A. In method II, we improved it by regarding each slender bar along the direction of wave propagation in region A as a tiny spring, and stiffness k as the parallel connection of all these tiny springs. Thus, using the integral technique, we have the new effective stiffness k for 2D case as

$$\begin{aligned} k &= 4C_{11}\int_0^{r_{core}}\left(\sqrt{r_{ext}^2 - x^2} - \sqrt{r_{core}^2 - x^2}\right)^{-1} dx \\ &= 2C_{11}\left[r_{core}/\sqrt{r_{ext}^2 - r_{core}^2} + \left(\pi r_{core}^2/2 + r_{ext}^2\arcsin(r_{core}/r_{ext})\right)/\left(r_{ext}^2 - r_{core}^2\right)\right] \end{aligned} \tag{6}$$

or for the 3D case as

$$k = 2C_{11} \iint_{(x^2+y^2)\le r_{core}^2} \left(\sqrt{r_{ext}^2 - x^2 - y^2} - \sqrt{r_{core}^2 - x^2 - y^2}\right)^{-1} dxdy$$
$$= 2C_{11} \int_0^{2\pi} \int_0^{r_{core}} \left(\sqrt{r_{ext}^2 - r^2} - \sqrt{r_{core}^2 - r^2}\right)^{-1} rdrd\theta = \frac{4\pi C_{11}}{3(r_{ext}^2 - r_{core}^2)} \left[r_{ext}^3 + r_{core}^3 - \left(r_{ext}^2 - r_{core}^2\right)^{3/2}\right] \quad (7)$$

Using method II and the analog models, we evaluate again the frequencies of the lowest band gap in 2D and 3D ternary LR PCs with different structural and material parameters (dashed lines in Figs. 5-9) and compared them with that calculated with the LM method (solid lines with dots in Figs. 5-9).

We can see that the frequencies evaluated with method II are much accurate than that evaluated with method I. However, there are still large mismatch according to the upper edges of the band gap. Especially in Fig. 7, when the density of the coating layer changes, the evaluated frequencies are changeless according to method I and II while the actual values are obviously in the reversed ratio with it. This is due to the ignorance of the density of coating layer in the calculation of parameters in the analog models.

We can found that when the LR PCs vibrate as the model in Fig. 4(e) (at the upper edge of the band gap), there exists a standing point that is immovable in the corresponding vibration modes. Thus the mass of the coating layer in region A can be divided according to the position of the standing point and add on m_1 and m_2 respectively. Based on the detailed vibration modes illustrated in Figs. 1(d) and 3(c), we can see that the coating layer in region B vibrates as the attachment of the host layer, which means that the mass of it can be add on m_2 directly. Thus in method III, the calculations of m_1 and m_2 are changed as

$$m_1 = m_{core} + m_A\alpha/(1+\alpha); \quad m_2 = m_{host} + m_B + m_A/(1+\alpha) \quad (8)$$

$$\alpha = m_2/m_1 = (m_A + m_B + m_{host})/(m_A + m_{core}) \quad (9)$$

For the 2D case, the mass of the coating layer in region A and B are

$$m_B = 2\rho_{\text{coating}} \int_{r_{core}}^{r_{ext}} 2\sqrt{r_{ext}^2 - x^2}\,dx = 2\rho_{\text{coating}} \left(\arccos(r_{core}/r_{ext})r_{ext}^2 - r_{core}\sqrt{r_{ext}^2 - r_{core}^2}\right)$$
$$m_A = \rho_{\text{coating}}\pi\left(r_{ext}^2 - r_{core}^2\right) - m_B \quad (10)$$

As for the 3D case,

$$m_B = 2\rho_{coating} \int_0^{2\pi} \int_{r_{core}}^{r_{ext}} \sqrt{r_{ext}^2 - r^2}\, rdrd\theta = \frac{4}{3}\rho_{coating}\pi(r_{ext}^2 - r_{core}^2)^{3/2}$$
$$m_A = (4/3)\rho_{coating}\pi\left(r_{ext}^3 - r_{core}^3\right) - m_B \quad (11)$$

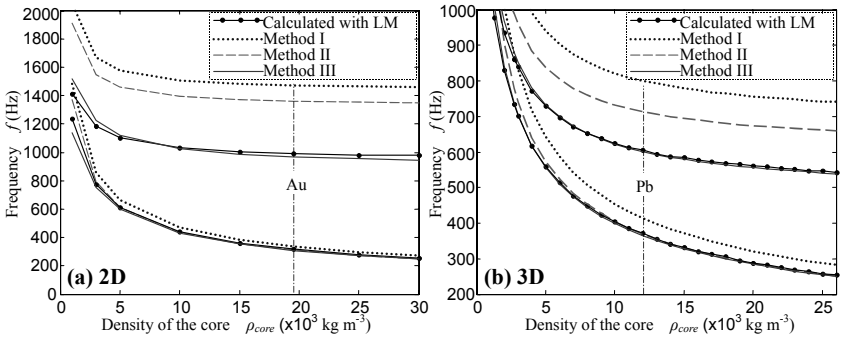

Figure 5 – Frequencies on the edges of the lowest band gap in the typical (a)2D and (b)3D ternary LR PCs for several densities of the core.

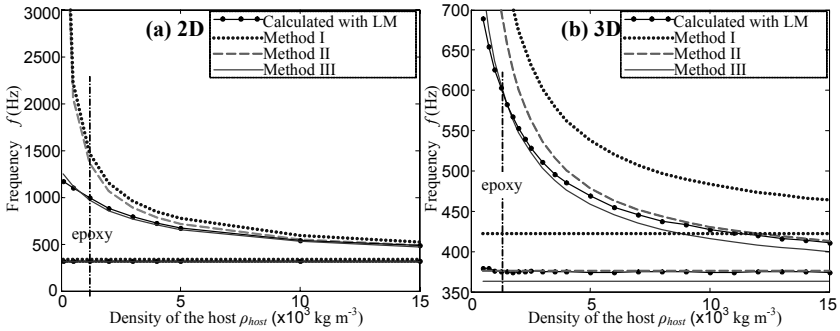

Figure 6 – Frequencies on the edges of the lowest band gap in the typical (a)2D and (b)3D ternary LR PCs for several densities of the host material.

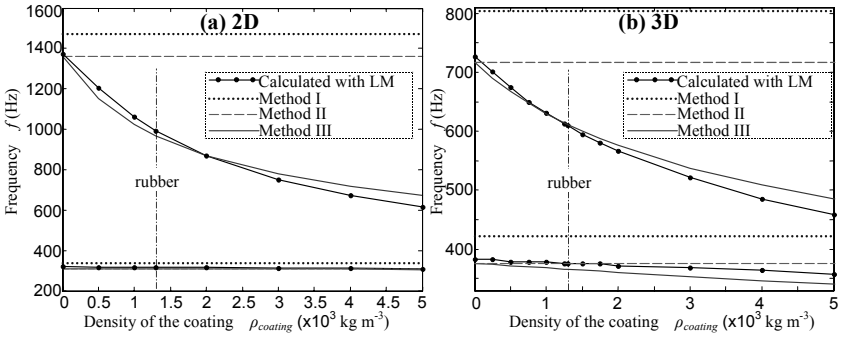

Figure 7 – Frequencies on the edges of the lowest band gap in the typical (a)2D and (b)3D ternary LR PCs for several densities of the coating material.

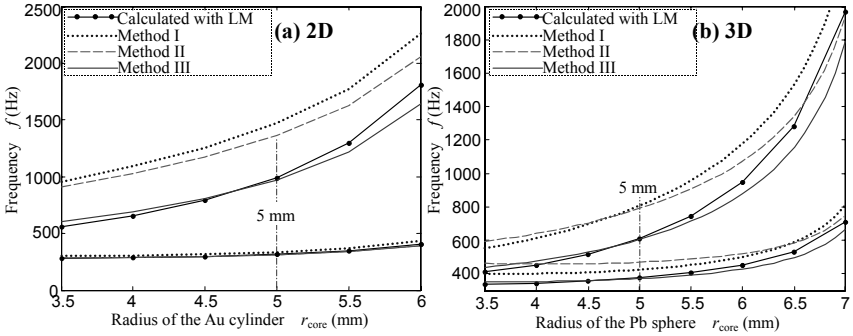

Figure 8 – Frequencies on the edges of the lowest band gap in the typical (a)2D and (b)3D ternary LR PCs for several radiuses of the core.

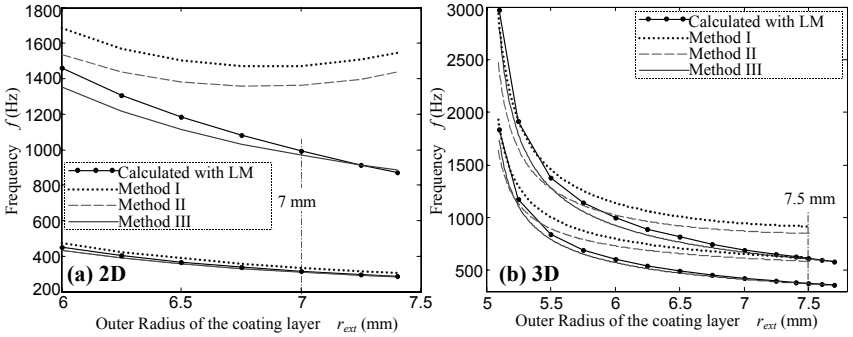

Figure 9 – Frequencies on the edges of the lowest band gap in the typical (a)2D and (b)3D ternary LR PCs for several outer radiuses of the coating layer.

The frequencies evaluated with method III and illustrated as solid lines in Figs. 5-9 match well with the theoretical results eventually on both the upper and the lower edge of the LR band gaps.

CONCLUSIONS

The vibration modes at the lower and the upper edges of lowest band gaps of both the two and three dimensional ternary locally resonant phononic crystals can be described with the "mass-spring-fixture" and the "mass-spring-mass" models respectively. The parameters of the models are given in a reasonable way based on the physical insight of the band gap mechanism. The analytical estimations with the models and the theoretical predictions with the lumped-mass method are in good agreement, especially for the upper edge of the locally resonant band gap. The proposal of these models are heuristic and helpful for better understanding of the locally resonant band gap mechanism as well as better estimation of the corresponding band edge frequencies. The latter make it possible for simple design of locally resonant gaps in phononic crystals, which is important for their applications as low frequency vibration/noise shelters.

REFERENCES

[1] M.S. Kushwaha, P. Halevi, L. Dobrzynski et al.,"Acoustic band structure of periodic elastic composites", Phys. Rev. Lett., 71, 2022-2025 (1993)
[2] Z. Liu, X. Zhang, Y. Mao et al.,"Locally resonant sonic materials", Science, 289, 1734-1736 (2000)
[3] R. Martínez-Sala, J. Sancho, J.V. Sánchez et al.,"Sound attenuation by sculpture", Nature (London), 378, 241 (1995)
[4] C. Goffaux, J. Sanchez-Dehesa, and P. Lambin,"Comparison of the sound attenuation efficiency of locally resonant materials and elastic band-gap structures", Phys. Rev. B, 70, 184302 (2004)
[5] C. Goffaux and J. Sánchez-Dehesa,"Two-dimensional phononic crystals studied using a variational method: Application to lattices of locally resonant materials", Phys. Rev. B, 67, 144301 (2003)
[6] C. Goffaux, J. Sánchez-Dehesa, A.L. Yeyati et al.,"Evidence of fano-like interference phenomena in locally resonant materials", Phys. Rev. Lett., 88, 225502 (2002)
[7] M. Hirsekorn,"Small-size sonic crystals with strong attenuation bands in the audible frequency range", Appl. Phys. Lett., 84, 3364-3366 (2004)
[8] M. Hirsekorn, P.P. Delsanto, N.K. Batra et al.,"Modelling and simulation of acoustic wave propagation in locally resonant sonic materials", Ultrasonics, 42, 231-235 (2004)
[9] J. Wen, G. Wang, Y. Liu et al.,"Lumped-mass method on calculation of elastic band gaps of one-dimensional phononic crystals", Acta Phys. Sin., 53, 3384-3388 (2004)
[10] G. Wang, J. Wen, and X. Wen,"Quasi-one-dimensional phononic crystals studied using the improved lumped-mass method: Application to locally resonant beams with flexural wave band gap", Phys. Rev. B, 71, 104302 (2005)
[11] G. Wang, X. Wen, J. Wen et al.,"Two-dimensional locally resonant phononic crystals with binary structures", Phys. Rev. Lett., 93, 154302 (2004)
[12] G. Wang, J. Wen, Y. Liu et al.,"Lumped-mass method for the study of band structure in two-dimensional phononic crystals", Phys. Rev. B, 69, 184302 (2004)
[13] Y. Cao, Z. Hou, and Y. Liu,"Convergence problem of plane-wave expansion method for phononic crystals", Phys. Lett. A, 327, 247-253 (2004)
[14] E. Yablonovitch,"Inhibited spontaneous emission in solid-state physics and electronics", Phys. Rev. Lett., 58, 2059-2062 (1987)
[15] S. John,"Strong localization of photons in certain disordered dielectric superlattices", Phys. Rev. Lett., 58, 2486-2489 (1987)